

Phase diagram of a random-anisotropy mixed-spin Ising model

A. P. Vieira, J. X. de Carvalho, and S. R. Salinas
Instituto de Física, Universidade de São Paulo
Caixa Postal 66318
05315-970, São Paulo, SP, Brazil
(October 31, 2018)

We investigate the phase diagram of a mixed spin- $\frac{1}{2}$ –spin-1 Ising system in the presence of quenched disordered anisotropy. We carry out a mean-field and a standard self-consistent Bethe–Peierls calculation. Depending on the amount of disorder, there appear novel transition lines and multicritical points. Also, we report some connections with a percolation problem and an exact result in one dimension.

05.50.+q, 64.60.Kw

I. INTRODUCTION

Apart from their relevance to the description of ferromagnetic materials, mixed-spin models are interesting from a purely theoretical point of view, being among the simplest models to exhibit tricritical behavior. So they are especially convenient for studying the effects of inhomogeneities on the phase diagrams and the multicritical behavior of magnetic systems. From a few exact^{1,2} and several approximate^{3–6} calculations, we now have a good picture of the phase diagrams of mixed spin- $\frac{1}{2}$ –spin-1 Ising models in the presence of a crystal field. Our aim in this work is to use this model Hamiltonian to investigate the effects of disorder on the location of the transition lines and the tricritical point.

The mixed-spin Ising model is described as a two-sublattice system, with spin variables $\sigma = \pm 1$ and $S = 0, \pm 1$, on the sites of sublattices A and B , respectively. Restricting the interactions to nearest-neighbors (belonging to different sublattices) and single-ion terms, the most general spin Hamiltonian in even spin space is written as

$$H = -J \sum_{\langle i \in A, j \in B \rangle} \sigma_i S_j + D \sum_{j \in B} S_j^2, \quad (1)$$

where the first sum is over nearest-neighbor pairs, the second sum is over the sites of sublattice B , and the parameter J is assumed to be positive (ferromagnetic exchange). For $D > 0$, the crystal field favors the $S_j = 0$ states; the competition between anisotropy and ferromagnetic exchange terms leads to the appearance of a tricritical point. It should be pointed out that one needs three parameters to describe the even space of the better known spin-1 Blume-Emery-Griffiths (BEG) model. In the present case of a mixed-spin Ising system, from the point of view of the calculations, the reduction of the analysis to a two-parameter space is a particularly attractive feature.

There are exact calculations for the thermodynamic functions associated with the model Hamiltonian given by Eq. (1) on a simple chain and on some three-

coordinated two-dimensional structures. On a honeycomb lattice, the problem can be mapped onto a spin- $\frac{1}{2}$ Ising model on a triangular lattice, which does not display a tricritical point.¹ This mixed-spin model can also be exactly solved on a Bethe lattice² (the deep interior of Cayley tree), leading to the same results of a recent cluster-variational calculation.⁶ The results on a Bethe lattice with coordination q indicate the absence of a tricritical point for $q < 5$, as confirmed by Migdal–Kadanoff renormalization-group calculations.⁴ In the infinite-coordination limit of the Bethe lattice, one regains the well-known results for the tricritical point displayed by the Curie–Weiss (mean-field) version of the model. An earlier approximate effective-field calculation⁷ predicted a tricritical point for $q \geq 4$, but this result has been recently challenged.^{8,9}

In order to analyze the effects of disorder, we consider the Hamiltonian

$$H = -J \sum_{\langle i \in A, j \in B \rangle} \sigma_i S_j + \sum_{j \in B} D_j S_j^2, \quad (2)$$

where $\{D_j\}$ is a set of independent, identically distributed random variables associated with the binary probability distribution

$$\wp(D_j) = p\delta(D_j) + (1-p)\delta(D_j - D). \quad (3)$$

With this choice of disorder, and for $D > qJ$, the ground state can be mapped onto a percolation problem in which the dilution affects the sites belonging to only one of the sublattices (corresponding to spin $S = 1$). This association is easy to see if we note that a uniform crystal field $D > qJ$ leads to $S_j = 0$ for all j , which breaks the connectivity between the spin-1/2 variables. The presence of a randomly located distribution of $D = 0$ crystal fields recovers that connectivity and, for sufficiently high values of p , leads to the formation of a percolating cluster. In the rather artificial case of annealed disorder, on the honeycomb lattice, there is also an exact solution¹⁰ for the thermodynamic properties of the mixed-spin model described by Eqs. (2) and (3). It is interesting to remark that this solution in the annealed case reproduces the

critical concentration of the percolation problem associated with the ground state of the model with quenched (frozen) disorder, which is equivalent to the usual percolation problem on the triangular lattice. For the physically more relevant case of quenched disorder, there are approximate calculations using an effective-field theory with correlations,¹¹ which point to the (expected) weakening of the tricritical behavior due to the presence of disorder.

In the present work, we first analyze the temperature–anisotropy ($T \times D$) phase diagram of the Curie–Weiss version (mean-field limit) of the spin Hamiltonian given by Eqs. (2) and (3). Depending on the concentration p , there appear novel transition lines and multicritical points. To include the effects of thermal fluctuations, we then resort to a standard self-consistent Bethe–Peierls approximation (which is analogous, in the case of the corresponding uniform model, to performing an exact Bethe-lattice calculation). In section II, we present the Curie–Weiss results. The Bethe–Peierls approximation is discussed in section III. In the appendices, we report

an exact solution in one-dimension as well as some low-temperature expansions to supplement the numerical results from the Bethe–Peierls approximation.

II. CURIE–WEISS VERSION

The Curie–Weiss version of the mixed-spin Ising model is given by the Hamiltonian

$$H = -\frac{2J}{N} \sum_{i \in A} \sigma_i \sum_{j \in B} S_j + \sum_{j \in B} D_j S_j^2, \quad (4)$$

where the sums are over all sites belonging to each one of the sublattices.

For a given disorder configuration $\{D_j\}$, we calculate the partition function by performing a partial trace over the set of spin variables $\{S_j\}$. In the thermodynamic limit, we use the saddle-point method and average over disorder to obtain the free energy functional

$$\Psi(\sigma) = -\frac{1}{2\beta} \left[\ln 2 - \frac{1}{2}(1 + \sigma) \ln(1 + \sigma) - \frac{1}{2}(1 - \sigma) \ln(1 - \sigma) \right] - \frac{1}{2\beta} \int \wp(D_B) \ln [1 + 2e^{-\beta D_B} \cosh(\beta J \sigma)] dD_B. \quad (5)$$

From the minimization of $\Psi(\sigma)$ with respect to σ , we have the A -sublattice magnetization,

$$\sigma = \tanh \left[\beta J \int \wp(D_B) \frac{2 \sinh(\beta J \sigma)}{e^{\beta D_B} + 2 \cosh(\beta J \sigma)} dD_B \right], \quad (6)$$

where the random variable D_B satisfies the probability distribution in Eq. (3). We can now calculate various expectation values. For example, we have

$$\begin{aligned} Q &= \int \wp(D_B) \langle S_B^2 \rangle dD_B \\ &= \int \wp(D_B) \frac{2 \cosh(\beta J \sigma)}{e^{\beta D_B} + 2 \cosh(\beta J \sigma)} dD_B. \end{aligned} \quad (7)$$

The critical line comes from the condition

$$\frac{\partial^2 \Psi}{\partial \sigma^2} \Big|_{\sigma=0} = 0 \implies e^\Delta = 2 \frac{(K-1) - \frac{1}{3} p K^2}{1 - \frac{2}{3} p K^2}, \quad (8)$$

where $\Delta = \beta D$ and $K = \beta J$. The thermodynamic stability of the critical line depends on the sign of the fourth derivative of $\Psi(\sigma)$ at $\sigma = 0$. There is then the possibility of a tricritical point, given by the additional condition

$$\frac{\partial^4 \Psi}{\partial \sigma^4} \Big|_{\sigma=0} = 0 \implies K^2 = \frac{3 + 9p + \sqrt{9 - 186p + 177p^2}}{8p}. \quad (9)$$

The stability of the tricritical point is determined by

$$\frac{\partial^6 \Psi}{\partial \sigma^6} \Big|_{\sigma=0} \geq 0 \implies p \leq p_m = 0.04485 \dots, \quad (10)$$

which means that the tricritical behavior is suppressed by disorder concentrations larger than approximately 4.5%.

In Fig. 1, we plot some $D \times T$ phase diagrams for a set of typical values of the concentration p . In the uniform case ($p = 0$), there is just a tricritical point, P_t . For $0 < p \leq p_m = 0.04485 \dots$, a tricritical point still exists (see Fig. 1, for $p = 0.04$). However, at low temperatures and sufficiently large values of D , there appears a low-density ($Q \rightarrow p$ as $T \rightarrow 0$) ferromagnetic phase, which we call ferro-II phase; at fixed values of D , an increase of temperature induces a second-order transition from the ferro-II to the paramagnetic phase. This transition is represented by a critical line that meets the first-order line at a critical end point, P_{ce} . This critical end point separates the first-order line into two distinct regions: (i) at higher temperatures, there are transitions between the usual, high-density ($Q \rightarrow 1$ as $T \rightarrow 0$) ferromagnetic phase (ferro-I) and the paramagnetic phase; (ii) at lower temperatures, the transitions are between the ferro-I and ferro-II phases, the first-order boundary ending at a finite-temperature critical point, P_{cs} .

For $p_m = 0.04485 \dots < p < 3/59 = 0.05084 \dots$, the tricritical point is replaced by a critical end point and a simple critical point, separated by a first-order transition line between the ferromagnetic phases (see inset in Fig. 1, for $p = 0.05$).

For $p \geq 3/59$, the critical line is fully stable (see Fig. 1, for $p = 0.08$). However, for $p \lesssim 0.1$, there still exists a small finite-temperature region where there are (first-order) transitions between the ferromagnetic phases.

III. BETHE–PEIERLS APPROXIMATION

To give an estimate of the effects of thermal fluctuations, which are not accounted for by the Curie–Weiss calculations, we now resort to a standard self-consistent Bethe–Peierls approximation. As the model is defined on a bipartite lattice, we have to consider two distinct clusters of coordination q (see Fig. 2). In one of them, which we call A , the central site is occupied by a spin $\sigma = \frac{1}{2}$, connected to q spins of the $S = 1$ type. In the other cluster, called B , there is a central $S = 1$ spin surrounded by q spin- $\frac{1}{2}$ variables. According to the standard prescription of the Bethe–Peierls approximation, we assume that the boundary spins of cluster A are under the action of an effective magnetic field \tilde{h}_B and an effective crystal field \tilde{D} , while the boundary spins of cluster B are in an effective magnetic field h_A . The crystal field acting on the central site of a cluster B is a random variable D_B . We

also consider external magnetic fields, h_A and h_B , acting on the central sites of clusters A and B , respectively.

For the sake of simplicity, we assume that the same effective crystal field \tilde{D} acts on all boundary spins of cluster A (and impose self-consistency between both thermal and disorder averages associated with the two clusters). In a more refined approach, we might introduce different effective crystal fields to mimic the extended disorder of real materials. However, we expect that, in the absence of external magnetic fields, the assumption of a single \tilde{D} is reasonable, at least in the paramagnetic phase, where there is no long-range order; in particular, we expect that the paramagnetic phase boundaries obtained by the two approaches are equivalent within the Bethe–Peierls approximation. We will see that this is indeed supported by the calculations.

The partition functions associated with the two clusters are given by

$$Z_A = e^{\gamma_A} \left[1 + 2e^{-\tilde{\Delta}} \cosh(\tilde{\gamma}_B + K) \right]^q + e^{-\gamma_A} \left[1 + 2e^{-\tilde{\Delta}} \cosh(\tilde{\gamma}_B - K) \right]^q \quad (11)$$

and

$$Z_B = [2 \cosh(\tilde{\gamma}_A)]^q + e^{-\Delta_B} \left\{ e^{\gamma_B} [2 \cosh(\tilde{\gamma}_A + K)]^q + e^{-\gamma_B} [2 \cosh(\tilde{\gamma}_A - K)]^q \right\}, \quad (12)$$

where $\gamma = \beta h$, $\Delta = \beta D$ and $K = \beta J$. The effective fields $\tilde{\gamma}_A$, $\tilde{\gamma}_B$ and $\tilde{\Delta}$ are determined by the consistency equations

$$\sigma = [\langle \sigma_j \rangle]_{\text{av}} = \frac{\partial \ln Z_A}{\partial \gamma_A} = \frac{1}{q} \int \wp(D_B) \frac{\partial \ln Z_B}{\partial \tilde{\gamma}_A} dD_B, \quad (13)$$

$$S = [\langle S_j \rangle]_{\text{av}} = \frac{1}{q} \frac{\partial \ln Z_A}{\partial \tilde{\gamma}_B} = \int \wp(D_B) \frac{\partial \ln Z_B}{\partial \gamma_B} dD_B, \quad (14)$$

and

$$Q = [\langle S_j^2 \rangle]_{\text{av}} = -\frac{1}{q} \frac{\partial \ln Z_A}{\partial \tilde{\Delta}} = -\int \wp(D_B) \frac{\partial \ln Z_B}{\partial \Delta_B} dD_B, \quad (15)$$

where $\langle \dots \rangle$ and $[\dots]_{\text{av}}$ indicate thermal and disorder averages, respectively. We point out that the introduction of the effective crystal field \tilde{D} is essential to achieve consistency between the equations for the two clusters.

In order to analyze the critical behavior, it is convenient to choose the magnetization σ , the temperature T , and the external fields h_B and D_B , as the independent thermodynamic variables. Thus, the external field h_A is written as a function of those variables, and the second-order transitions in zero external field ($h_A = h_B = 0$) are given by

$$\left. \frac{\partial \gamma_A}{\partial \sigma} \right|_{\sigma=0} = 0 \implies Q_0 = \frac{1}{(q-1)^2 \tanh^2 K}, \quad (16)$$

where the derivative is taken for fixed values of the remaining independent variables, and

$$Q_0 \equiv Q|_{\sigma=0} = \int \wp(D_B) \frac{2 \cosh^q K}{e^{\Delta_B} + 2 \cosh^q K} dD_B. \quad (17)$$

To calculate the derivative in Eq. (16), we take the (implicit) derivative of the consistency equations with respect to σ , imposing the condition $\sigma = 0$ and eliminating the derivatives involving S , Q and the effective fields. Also, for $\sigma = 0$, we have $S = \tilde{\gamma}_A = \tilde{\gamma}_B = 0$, since those variables are odd functions of σ for $h_A = h_B = 0$. Thus, the consistency equation for Q leads to

$$\tilde{\Delta} \Big|_{\sigma=0} = \ln \left(2 \frac{1 - Q_0}{Q_0} \cosh K \right), \quad (18)$$

and the final result is

$$\left. \frac{\partial \tilde{\gamma}_A}{\partial \sigma} \right|_{\sigma=0} = \frac{1 + [2(q-1) - q^2] V_0 + (q-1)^2 V_0^2}{1 + (q-2)V_0 + (q-1)^2 V_0^2}, \quad (19)$$

where $V_0 = Q_0 \tanh^2 K$. For $q = 2$, Eq. (19) reproduces the exact one-dimensional expression for the A -sublattice susceptibility (see Appendix A). In fact, for $q = 2$, it is not difficult to check that we regain all the exact one-dimensional results.

It is easy to see that, in the uniform case, corresponding to $\wp(D_B) = \delta(D_B - D)$, the critical line is given by

$$\Delta = \ln \left\{ 2 (\cosh K)^{q-2} [q(q-2) \cosh^2 K - (q-1)^2] \right\}, \quad (20)$$

in agreement with the results from the Bethe-lattice² and the cluster-variational⁶ calculations.

Using the binary distribution in Eq. (3), we obtain

$$Q_0 = p \frac{2 \cosh^q K}{1 + 2 \cosh^q K} + (1-p) \frac{2 \cosh^q K}{e^{\Delta} + 2 \cosh^q K}. \quad (21)$$

Therefore, the critical line is given by

$$e^{\Delta} = 2 \frac{(1-p) - \phi(K)}{\phi(K)} \cosh^q K, \quad (22)$$

where

$$\phi(K) = \frac{1}{(q-1)^2} \frac{\cosh^2 K}{\cosh^2 K - 1} - p \frac{2 \cosh^q K}{1 + 2 \cosh^q K}. \quad (23)$$

In the $T \rightarrow 0$ ($K \rightarrow \infty$) limit, we have

$$e^{\Delta} \simeq \frac{e^{qK}}{2^{q-1}} \frac{(q-1)^2 - 1}{1 - p(q-1)^2}, \quad (24)$$

which has a real solution for Δ if

$$1 - p(q-1)^2 > 0 \implies p < p_{cr} = \frac{1}{(q-1)^2}. \quad (25)$$

This last result should be anticipated for a Bethe lattice, as we can see from the following arguments. Consider a Cayley tree where the sites belonging to every other shell, say those on odd-numbered shells, are occupied with probability p , while the remaining sites are always occupied. If q is the coordination of the tree, the average number of paths from the root (shell 0) to the first shell is given by $p(q-1)$, while we have $p(q-1)^2$ paths from there to the second shell. According to this reasoning, the average number of paths from the root to the $(2n)$ th shell is given by $p^n(q-1)^{2n}$. In order to have at least one path to the surface of the tree ($n \rightarrow \infty$), it is required that $p(q-1)^2 \geq 1$, which is just the condition in Eq. (25). This result, together with the reproduction of the exact one-dimensional solution, would suggest that the present treatment also gives exact results on the Bethe lattice even in the presence of disorder. However, as remarked in previous similar treatments,^{12,13} this works for the paramagnetic phase only, because only then it is correct to assume that all boundary sites are under the action of the same (zero) effective field. The existence of a percolating cluster, which we do not take into account in this treatment, prevents this approximation from still giving correct results for the ordered phases.

We now consider Eq. (22), in the infinite coordination limit ($q \rightarrow \infty$, $K \rightarrow 0$, $qK = \tilde{K}$). We then have

$$e^{\Delta} = 2 \frac{(\tilde{K} - 1) - \frac{1}{3} p \tilde{K}^2}{1 - \frac{2}{3} p \tilde{K}^2}, \quad (26)$$

which agrees with Eq. (8) for the Curie-Weiss version of the model.

The tricritical points are determined by Eq. (16) supplemented by the condition

$$\left. \frac{\partial^3 \gamma_A}{\partial \sigma^3} \right|_{\sigma=0} = 0,$$

which is equivalent to

$$\frac{2q^2 - 10q + 6}{(q-1)^5 \tanh^2 K} + 3qW_0 \tanh^2 K = \frac{(q-2)(q-3)}{(q-1)^3}, \quad (27)$$

where W_0 is given by

$$W_0 = \int \wp(D_B) \left(\frac{2 \cosh^q K}{e^{\Delta_B} + 2 \cosh^q K} \right)^2 dD_B. \quad (28)$$

The tricritical points are stable if

$$\left. \frac{\partial^5 \gamma_A}{\partial \sigma^5} \right|_{\sigma=0} > 0.$$

To calculate this derivative, we again take implicit derivatives of the consistency equations (up to fifth order) with respect to σ , at $\sigma = 0$, and eliminate all derivatives involving S , Q and the effective fields. Unlike the previous analysis, we have not been able to obtain closed-form expressions for the stability condition of the tricritical point, but it is not difficult to perform a number of numerical calculations.

For the uniform model, we have $W_0 = Q_0^2$. Therefore, Eq. (27) takes the form

$$\tanh K = \frac{1}{q-1} \sqrt{\frac{5q-3}{q-3}}, \quad (29)$$

which is again identical to the result obtained from the Bethe-lattice² and the cluster-variational⁶ calculations. Notice that this equation has real solutions only if $q > 4.561553 \dots$. Thus, the Bethe-Peierls approximation does not predict a tricritical point for the square lattice ($q = 4$).

For the binary distribution in Eq. (3), we have

$$W_0 = Q_0^2 \left[1 + \frac{p}{1-p} \left(1 - \frac{1}{Q_0} \frac{2 \cosh^q K}{1 + 2 \cosh^q K} \right)^2 \right]. \quad (30)$$

In the infinite-coordination limit we can write

$$W_0 = \frac{1}{\tilde{K}^4} \left[1 + \frac{p}{1-p} \left(1 - \frac{2}{3} \tilde{K}^2 \right)^2 \right], \quad (31)$$

which leads to the equation

$$\tilde{K}^2 - 3 \left[1 + \frac{p}{1-p} \left(1 - \frac{4}{3} \tilde{K}^2 + \frac{4}{9} \tilde{K}^4 \right) \right] - 2 = 0, \quad (32)$$

at the tricritical point. Indeed, one of the solutions of this equation corresponds to Eq. (9), for the Curie–Weiss version of the model, while the other solution represents a thermodynamically unstable situation.

In Table I, for various values of the coordination number q , and using the binary distribution given by Eq. (3), we give the corresponding values of the concentration p_m , at which the tricritical point becomes unstable, and the critical percolation concentration p_{cr} . We see that, for $q \leq 10$, the tricritical behavior is suppressed for $p_m < p_{cr}$, while, for $q \geq 11$, that suppression occurs for $p_m > p_{cr}$. As shown in Table I, p_m increases with q , which indicates that disorder is more effective for small coordination numbers.

As the effects of binary disorder strongly depend on the coordination, we now discuss the phase diagrams for the typical cases.

For $q = 3$ and 4, there are no tricritical points. The $D \times T$ phase diagram displays just a fully stable critical line. The main effect of disorder is to make the paramagnetic phase unstable at $T = 0$, regardless of the value of D , for p larger than the critical percolation concentration p_{cr} . The phase diagrams in Fig. 3, for $q = 3$, are in qualitative agreement with the exact results for the honeycomb lattice (which is also three-coordinated) under annealed disorder.¹⁰ At $T = 0$, there is even quantitative agreement with the value of the critical crystal field at p_{cr} , given by $D_{cr} = 5J/3$, although of course this agreement does not extend to the value of p_{cr} itself. Our results for $q = 3$ and $q = 4$ are also in qualitative agreement with those obtained by a real-space renormalization-group approach for the two-dimensional Blume–Emery–Griffiths model in a random crystal field.¹⁴

For $5 \leq q \leq 10$, the concentration p_m above which the tricritical point becomes unstable is lower than p_{cr} . For $p < p_m$, disorder depresses the tricritical temperature, and shortens the first-order transition line. For $p_m < p < p_{cr}$, the tricritical point is replaced by a critical end point, P_{ce} , and a simple critical point, P_{cs} , as in the Curie–Weiss version of the model. However, the paramagnetic phase is stable at $T = 0$ if $D > qJ$, and the first-order line reaches $D = qJ$ at $T = 0$. As p increases, first the critical end point P_{ce} and then the simple critical point P_{cs} reach the $T = 0$ axis, at values of p which can be determined by a low-temperature expansion of the consistency equations (see Appendix B). In Fig. 4, we plot the $D \times T$ phase diagram for $q = 6$ and $p = 0.011$. To determine the first-order lines shown in that figure, we numerically solve the consistency equations to obtain the conditions $h_A(\sigma_1) = h_A(\sigma_2) = 0$ and

$$\int_{\sigma_1}^{\sigma_2} h_A(\sigma) d\sigma = 0, \quad (33)$$

which correspond to a Maxwell construction.

For $q \geq 11$, we have $p_m > p_{cr}$, so the behavior of the system is quite similar to the predictions of the Curie–

Weiss version of the model.

IV. CONCLUSIONS

We performed detailed calculations for the phase diagram of a random-anisotropy mixed-spin Ising model both in the mean-field limit (Curie–Weiss version of the model), in which thermal fluctuations are neglected, and according to a standard self-consistent Bethe–Peierls approximation (which turns out to be exact in one dimension). For a binary distribution of crystal fields, we obtained closed-form expressions for the critical lines and the location of the tricritical points. Depending on the concentration p , the mean-field results for the $D \times T$ phase diagrams predict novel first-order lines and multicritical points (besides a ferromagnetic region, for all values of the crystal field, extending down to the lowest temperatures). The Bethe–Peierls approximation shows that this additional ferromagnetic region is suppressed for concentrations below a certain percolation threshold. Also, the Bethe–Peierls results point out to the absence of a tricritical behavior for lattices with coordination $q \leq 4$. All results reported in this paper are in agreement with general predictions for the effects of disorder on first-order transitions and multicritical points (for a recent review, see a paper by Cardy¹⁵).

ACKNOWLEDGMENTS

We thank T. A. S. Haddad for useful discussions. This work was partially financed by the Brazilian agencies FAPESP and CNPq.

APPENDIX A: EXACT SOLUTION IN ONE-DIMENSION

For an open chain with $N + 1$ sites (N even), and in zero external field, the Hamiltonian of the mixed-spin Ising model can be written as

$$H = -J \sum_{j=1}^{N/2} (\sigma_j S_j + S_j \sigma_{j+1}) + \sum_{j=1}^{N/2} D_j S_j^2. \quad (A1)$$

Given a disorder configuration $\{D\} = \{D_1, \dots, D_{N/2}\}$, we perform a partial trace over the spin variables $\{S_j\}$ to write

$$\begin{aligned} Z\{D\} &= \sum_{\{\sigma\}} \sum_{\{S\}} e^{-\beta H} \\ &= \sum_{\{\sigma\}} \prod_{j=1}^{N/2} \{1 + 2e^{-\Delta_j} \cosh[K(\sigma_j + \sigma_{j+1})]\}, \quad (A2) \end{aligned}$$

where $K = \beta J$ and $\Delta_j = \beta D_j$. Introducing a prefactor A_j ,

$$A_j^2 = (1 + 2e^{-\Delta_j}) [1 + 2e^{-\Delta_j} \cosh(2K)] \quad (\text{A3})$$

and an effective interaction \tilde{K}_j , such that

$$e^{2\tilde{K}_j} = \frac{1 + 2e^{-\Delta_j} \cosh(2K)}{1 + 2e^{-\Delta_j}}, \quad (\text{A4})$$

the partition function can be written as the factorized form

$$\begin{aligned} Z\{D\} &= \sum_{\{\sigma\}} \prod_{j=1}^{N/2} A_j e^{\tilde{K}_j \sigma_j \sigma_{j+1}} \\ &= \prod_{j=1}^{N/2} 2 [1 + 2e^{-\Delta_j} \cosh^2 K]. \end{aligned} \quad (\text{A5})$$

From Eq. (A5), we obtain the thermal average

$$\langle S_j^2 \rangle_{\{D\}} = -\frac{\partial \ln Z}{\partial \Delta_j} = \frac{2e^{-\Delta_j} \cosh^2 K}{1 + 2e^{-\Delta_j} \cosh^2 K}, \quad (\text{A6})$$

which depends on the value of the crystal field on the j th site only. Since we are considering a nearest-neighbor one-dimensional model in zero field, the thermal averages $\langle S_j \rangle$ and $\langle \sigma_j \rangle$ are zero. Performing the disorder average, we obtain the expectation value

$$Q = \int \langle S_j^2 \rangle \prod_{i=1}^{N/2} \wp(D_i) dD_i = \int \wp(D_j) \langle S_j^2 \rangle_{\{D\}} dD_j. \quad (\text{A7})$$

For a given disorder configuration, the magnetic susceptibilities of the σ and S sublattices are given by

$$\chi_\sigma\{D\} = \frac{1}{T} \lim_{N \rightarrow \infty} \frac{2}{N+2} \sum_{j=1}^{\frac{N}{2}+1} \sum_{k=1}^{\frac{N}{2}+1} \langle \sigma_j \sigma_k \rangle_{\{D\}} \quad (\text{A8})$$

and

$$\chi_s\{D\} = \frac{1}{T} \lim_{N \rightarrow \infty} \frac{2}{N} \sum_{j=1}^{N/2} \sum_{k=1}^{N/2} \langle S_j S_k \rangle_{\{D\}}. \quad (\text{A9})$$

The two-spin correlation functions,

$$\langle \sigma_j \sigma_k \rangle_{\{D\}} = \frac{1}{Z\{D\}} \sum_{\{\sigma\}} \sum_{\{S\}} \sigma_j \sigma_k e^{-\beta H} \quad (\text{A10})$$

and

$$\langle S_j S_k \rangle_{\{D\}} = \frac{1}{Z\{D\}} \sum_{\{\sigma\}} \sum_{\{S\}} S_j S_k e^{-\beta H}, \quad (\text{A11})$$

can be calculated if we introduce the transformation

$$\tau_j = \sigma_j \sigma_{j+1} \quad \text{with} \quad \tau_0 = \sigma_1. \quad (\text{A12})$$

After some algebraic manipulations, for $j < k$, we have

$$\langle \sigma_j \sigma_k \rangle_{\{D\}} = \prod_{i=j}^{k-1} \frac{2 \sinh^2 K}{e^{\Delta_i} + 2 \cosh^2 K} \quad (\text{A13})$$

and

$$\begin{aligned} \langle S_j S_k \rangle_{\{D\}} &= \left(\prod_{i=j,k} \frac{\sinh 2K}{e^{\Delta_i} + 2 \cosh^2 K} \right) \\ &\times \prod_{i=j+1}^{k-1} \frac{2 \sinh^2 K}{e^{\Delta_i} + 2 \cosh^2 K}, \end{aligned} \quad (\text{A14})$$

from which we obtain the expectation values

$$\begin{aligned} g_\sigma(|k-j|) &= \int \langle \sigma_j \sigma_k \rangle_{\{D\}} \prod_{i=1}^{N/2} \wp(D_i) dD_i \\ &= (Q \tanh^2 K)^{|k-j|} \end{aligned} \quad (\text{A15})$$

and

$$\begin{aligned} g_s(|k-j|) &= \int \langle S_j S_k \rangle_{\{D\}} \prod_{i=1}^{N/2} \wp(D_i) dD_i \\ &= Q (Q \tanh^2 K)^{|k-j|}, \end{aligned} \quad (\text{A16})$$

which depend on the distance between sites j and k . The expectation values of the susceptibilities are given by

$$[\chi_\sigma]_{\text{av}} = \frac{1}{T} \left[1 + 2 \sum_{r=1}^{\infty} g_\sigma(r) \right] = \frac{1}{T} \frac{1 + Q \tanh^2 K}{1 - Q \tanh^2 K} \quad (\text{A17})$$

and

$$[\chi_s]_{\text{av}} = \frac{1}{T} \left[Q + 2 \sum_{r=1}^{\infty} g_s(r) \right] = \frac{Q}{T} \frac{1 + Q \tanh^2 K}{1 - Q \tanh^2 K}, \quad (\text{A18})$$

where Q is determined by Eq. (A7).

APPENDIX B: LOW-TEMPERATURE EXPANSION

For the binary distribution, in the low-temperature limit ($K = \beta J \gg 1$), if we neglect terms of order $\exp(-2K)$ and higher, the consistency equations (13)-(15) for cluster A lead to the expressions

$$\gamma_A = \frac{1}{2} \ln \frac{1+\sigma}{1-\sigma} + \frac{q}{2} \ln \frac{1-C_+}{1-C_-}, \quad (\text{B1})$$

$$S = \frac{1+\sigma}{2} C_+ - \frac{1-\sigma}{2} C_-, \quad (\text{B2})$$

and

$$Q = \frac{1+\sigma}{2}C_+ + \frac{1-\sigma}{2}C_-, \quad (\text{B3})$$

where

$$C_{\pm} = \frac{e^{\pm\tilde{\gamma}_B}}{e^{\Delta-K} + e^{\pm\tilde{\gamma}_B}}. \quad (\text{B4})$$

For cluster B , we have

$$\sigma = p \tanh(q\tilde{\gamma}_A) + (1-p) \frac{\tau(\tilde{\gamma}_A) \tanh(\tilde{\gamma}_A) + \delta \tanh(q\tilde{\gamma}_A)}{\tau(\tilde{\gamma}_A) + \delta}, \quad (\text{B5})$$

$$S = p \tanh(q\tilde{\gamma}_A) + (1-p) \frac{\delta}{\tau(\tilde{\gamma}_A) + \delta} \tanh(\tilde{\gamma}_A), \quad (\text{B6})$$

$$Q = p + (1-p) \frac{\delta}{\tau(\tilde{\gamma}_A) + \delta}, \quad (\text{B7})$$

where

$$\delta = \exp(qK - \Delta), \quad (\text{B8})$$

and

$$\tau(x) = \frac{2^q}{(1 + \tanh x)^q + (1 - \tanh x)^q}. \quad (\text{B9})$$

Solving Eqs. (B2) and (B3) for C_{\pm} in terms of σ , S and Q , and using Eqs. (B5)-(B7), we can write Eq. (B1) in the form

$$\gamma_A(\sigma) = \frac{1-q}{2} \ln \frac{1+\sigma}{1-\sigma} + q\tilde{\gamma}_A(\sigma), \quad (\text{B10})$$

where $\tilde{\gamma}_A(\sigma)$ is determined from the solution of Eq. (B5). Notice that, according to Eqs. (B10) and (B5), $\gamma_A(\sigma)$ and $\tilde{\gamma}_A(\sigma)$ depend on the temperature through the parameter δ only. As $T \rightarrow 0$, this parameter goes to zero (if $D > qJ$), or infinity (if $D < qJ$), except in the vicinity of the point P_0 with coordinates $D = qJ$, and $T = 0$, where δ can assume any value.

Since the equation of state (B10) becomes asymptotically exact as $T \rightarrow 0$, it can be used to determine the values of p at which the critical end point and the simple critical point reach P_0 , and thus disappear. To do that calculation, we impose the conditions

$$\gamma_A(\sigma_e) = \left. \frac{\partial \gamma_A}{\partial \sigma} \right|_{\sigma=\sigma_e} = \left. \frac{\partial^2 \gamma_A}{\partial \sigma^2} \right|_{\sigma=\sigma_e} = 0, \quad (\text{B11})$$

from which we obtain the values of σ_e , δ_e and p_e at which the critical end point reaches P_0 , and the conditions

$$\gamma_A(\sigma_s) = \left. \frac{\partial \gamma_A}{\partial \sigma} \right|_{\sigma=\sigma_s} = \int_0^{\sigma_s} \gamma_A(\sigma) d\sigma = 0, \quad (\text{B12})$$

which give the corresponding values σ_s , δ_s and p_s for the simple critical point.

- ¹ L. L. Gonçalves, Phys. Scr. **32**, 248 (1985).
- ² N. R. da Silva and S. R. Salinas, Phys. Rev. B **44**, 852 (1991).
- ³ G.-M. Zhang and C.-Z. Yang, Phys. Rev. B **48**, 9452 (1993)
- ⁴ S. G. A. Quadros and S. R. Salinas, Physica A **206**, 479 (1994).
- ⁵ G. M. Buendía and M. A. Novotny, J. Phys.: Condens. Matter **9**, 5951 (1997).
- ⁶ J. W. Tucker, J. Magn. Magn. Mater. **195**, 733 (1999).
- ⁷ T. Kaneyoshi, J. Phys. Soc. Jpn. **56**, 2675 (1987).
- ⁸ A. Bobák and M. Jurčičin, Physica A **240**, 647 (1997).
- ⁹ A. L. de Lima, B. D. Stošić, and I. P. Fittipaldi, J. Magn. Magn. Mater., to be published.
- ¹⁰ J. R. Gonçalves and L. L. Gonçalves, J. Magn. Magn. Mater. **104-107**, 261 (1992).
- ¹¹ T. Kaneyoshi, Physica A **153**, 556 (1988).
- ¹² G. M. Bell, J. Phys. C: Solid State Phys. **8**, 669 (1975).
- ¹³ A. P. Young, J. Phys. C: Solid State Phys. **9**, 2103 (1976).
- ¹⁴ N. S. Branco, Phys. Rev. B **60**, 1033 (1999).
- ¹⁵ J. L. Cardy, Physica A **263**, 215 (1999).

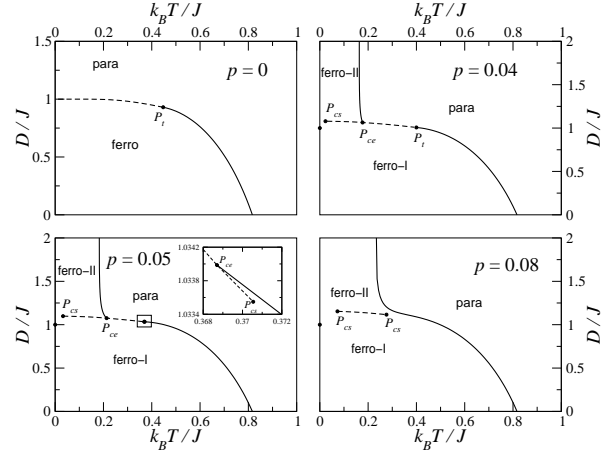


FIG. 1. Phase diagrams of the Curie–Weiss version for typical values of the disorder concentration p .

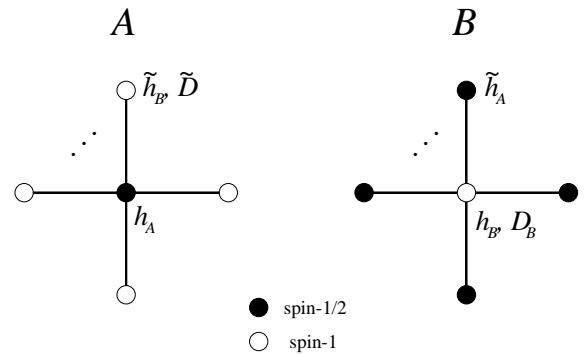


FIG. 2. Clusters used in the Bethe–Peierls approximation.

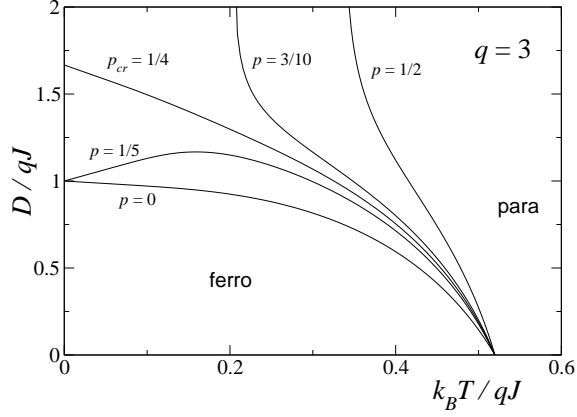


FIG. 3. Phase diagrams for coordination $q = 3$ according to the Bethe–Peierls approximation.

FIG. 4. Phase diagram for coordination $q = 6$ and disorder concentration $p = 0.011$ according to the Bethe–Peierls approximation.

TABLE I. Values of the critical percolation concentration p_{cr} and the concentration p_m at which the tricritical point becomes unstable, as functions of the coordination q in the Bethe–Peierls approximation.

q	p_{cr}	p_m
5	6.25×10^{-2}	7.4161×10^{-4}
6	4×10^{-2}	2.0454×10^{-3}
10	1.2346×10^{-2}	9.8265×10^{-3}
11	1×10^{-2}	1.1665×10^{-2}
20	2.7701×10^{-3}	2.3001×10^{-2}
100	1.0203×10^{-4}	3.9707×10^{-2}
∞	0	4.4850×10^{-2}

